J. Fluid Mech. (2011), *vol.* 675, *pp.* 529–539. © Cambridge University Press 2011
doi:10.1017/S0022112011000681

Solid landslide generated waves

YANG WANG[1,2], PHILIP L.-F. LIU[1,3]† AND CHIANG C. MEI[1,4]

[1]School of Civil and Environmental Engineering, Cornell University, Ithaca, NY 14853-3501, USA
[2]Department of Hydraulic Engineering, Tsinghua University, Beijing 100084, China
[3]Institute of Hydrological and Oceanic Sciences, National Central University, Jhongli 32001, Taiwan
[4]Department of Civil and Environmental Engineering, MIT, Cambridge, MA 02139-4307, USA

(Received 2 August 2010; revised 2 February 2011; accepted 6 February 2011;
first published online 25 March 2011)

Theoretical formulation describing the wave generation by a slender solid landslide is presented. The slide motion is coupled with the surface wave dynamics and both the fluid viscous (lubricative) resistance and the solid friction are considered.

Numerical results are obtained for a cosine function shape slide. Numerical results show clearly the importance of the dynamic nonlinear coupling. The effects of lubricative resistance, solid friction, initial landslide speed and the slide height are discussed.

Key words: coastal engineering, shallow water flows, surface gravity waves

1. Introduction

Aerial landslides can generate large water waves and cause devastating damage to coastal communities. For example, on July 9, 1958, an M 7.9 earthquake triggered a huge landslide on the bank of Lituya Bay, Alaska, which generated large waves that ran up to the opposite side of the bay. The maximum run-up height was about 525 m. There are many other reported landslide generated tsunami hazards (e.g. Synolakis *et al.* 2002; Tinti *et al.* 2003).

Numerous theoretical and numerical modelling research on the aerial and submerged landslide generated waves exist (e.g. Pelinovsky & Poplavsky 1996; Lynett & Liu 2002, 2005; Watts *et al.* 2003; Liu, Lynett & Synolakis 2003; Liu *et al.* 2005; Sammarco & Renzi 2008; Renzi & Sammarco 2010). In all these models, the slide geometry and its motion are prescribed *a priori*, and therefore, the interactions between the land mass and its ambient flows are ignored. It is our intention to explore the importance of these interactions on the generated waves. To this end, the solid friction between the bottom of the slide and the beach face, the fluid viscous (lubrication) friction and the pressure force on the wetted surface of the slide are all included in the formulation of slide motion. However, we focus attention only to a laboratory model of a solid sliding on a smooth slope where a thin gap of uniform thickness δ exists between the beach face and the bottom of the sliding solid, maintained by sparsely populated discrete asperities. Airy's nonlinear equations for long waves in shallow water will be used.

The formulation of the nonlinear coupling problem is presented in § 2. Assumptions and simplifications are stated. The analytical solution for the flows in the gap is given in § 3. Numerical results for a falling solid slide of cosine profile are then shown in

† Email address for correspondence: Philip.liu@cornell.edu

https://doi.org/10.1017/S0022112011000681 Published online by Cambridge University Press

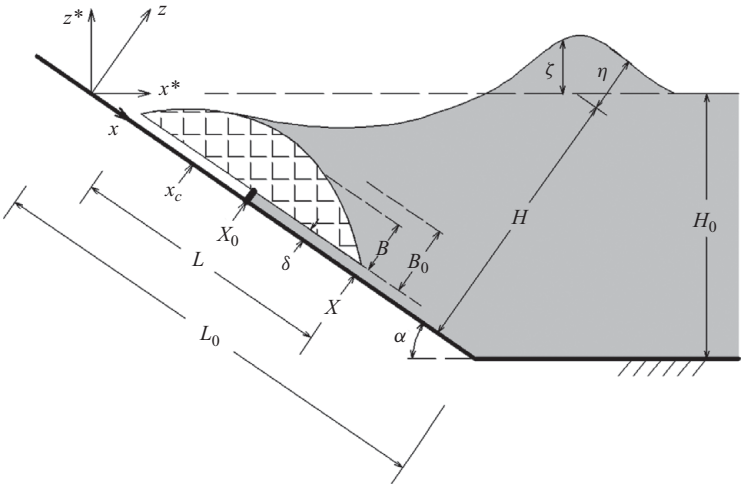


FIGURE 1. Definition sketch.

§4. The effects of lubricative resistance, solid friction, initial landslide speed and the slide height are discussed.

2. Formulation

We consider a solid slide with a prescribed shape and mass (M) sliding down a constant slope (α), which is truncated and connected to a constant depth as shown in figure 1. Using the coordinate system (x^*, z^*), in which x^* is pointing in the offshore horizontal direction and z^* the vertical upward direction, the still water depth can be expressed as $z^* = -x^* \tan\alpha$ for $x^* \leqslant L_0$. For convenience, we use another coordinate system (x, z) where x-axis coincides with the unperturbed beach face and z-axis is normal to the beach face (see figure 1). Thus, $x^* = x\ \cos\alpha + z\ \sin\alpha$ and $z^* = z\ \cos\alpha - x\ \sin\alpha$.

At $t = 0$, the head of the slide reaches the still water shoreline. The shape of the slide is fixed, $z = B(x, t)$. Denoting L as the length of the base and B_0 as the maximum thickness of the slide, we limit our attention to the case of $L \gg B_0$. However, since the water depth is very shallow near the shoreline, the thickness of the slide is comparable to water depth.

Let $x = X(t)$ be the position of the head of slide with $X(0) = 0$. The shape of the slide can be expressed as $z = B(\xi)$ in terms of a local body coordinate,

$$\xi = x + [L - X(t)]. \tag{2.1}$$

We start the analysis as the head of the solid slide enters water with a given velocity,

$$X(0) = 0, \quad \frac{\mathrm{d}X}{\mathrm{d}t} = U_s, \quad \text{at } t = 0. \tag{2.2}$$

2.1. *Slide dynamics*

Two types of resistant force are considered: solid friction acting on the asperities and fluid lubricative resistance in the gap. For simplicity, we shall neglect the slide movement in the direction normal to the beach face and the fluid friction on the top surface of the slide, which are small.

https://doi.org/10.1017/S0022112011000681 Published online by Cambridge University Press

Let F_s denote the solid friction and F_h denote the lubricative resistance. During the entry period when the slide is partially submerged, the shoreline at the tail of the gap is at $x = X_0(t)$ from the initial position, i.e. $X_0(0) = 0$. The lubricative resistance is

$$F_h = \int_{X_0}^{X} \mathrm{d}x \left[\mu \frac{\partial u_g}{\partial z} \right]_{z=\delta}, \tag{2.3}$$

where μ is the viscosity of the water and u_g is the water velocity inside the gap, for which the analysis is given in § 3. The solid friction force can be expressed as

$$F_s = f_s \left(Mg \cos\alpha + \int_{x_c}^{X} p_b \, \mathrm{d}x - \int_{X_0}^{X} p \, \mathrm{d}x \right), \tag{2.4}$$

where M is the mass of the solid slide, g is the gravity acceleration, and f_s is the solid frictional coefficient. Note that p represents the fluid pressure in the gap along the wetted bottom of the slide and p_b represents the water pressure along the upper wetted surface of the slide,

$$p_b(x, t) = \rho g \cos\alpha \left[\eta(x, t) + H - B(\xi) \right]. \tag{2.5}$$

Furthermore, $x_c(t)$ denotes the x-coordinate of the moving shoreline (see figure 1) and can be found by solving

$$\eta(x_c, t) + H(x_c) - B(x_c, t) = 0, \tag{2.6}$$

where $z = \eta(x, t)$ is the free surface elevation.

The force balance in the direction of slide motion yields

$$M\ddot{X} = Mg \sin\alpha + \int_{L-\xi_c}^{L} p_b(x, t) \frac{\partial B}{\partial \xi} \mathrm{d}\xi - F_s - F_h, \tag{2.7}$$

where $\ddot{X}$ denotes the second time derivatives of the slide displacement and $\xi_c(t)$ is the wetted length of the sliding mass defined as $\xi_c = x_c(t) + [L - X(t)]$. Clearly, the slide motion is coupled with the flow dynamics. The relative importance of solid friction and lubricative resistance will be discussed in § 4.

2.2. *Water wave generation*

As the slide enters the water body, waves are generated. The wave motions can be described by the Airy nonlinear long wave theory. Thus, the continuity equation is written in terms of the depth averaged velocity, u, and the free surface elevation, η, as

$$\frac{\partial \eta}{\partial t} + \frac{\partial}{\partial x} \left[(\eta + H - B(\xi)) u \right] = \frac{\partial B}{\partial t}. \tag{2.8}$$

The momentum equation in the direction of slide movement is

$$\frac{\partial u}{\partial t} + u \frac{\partial u}{\partial x} = -g \cos\alpha \frac{\partial \eta}{\partial x}. \tag{2.9}$$

The initial conditions at $t = 0$ are: $\eta(x, 0) = u(x, 0) = 0$.

3. Viscous resistance along the bottom of slide

In the gap, $0 < z < \delta$, the momentum equation of flow motions in the x-direction can be written as

$$\frac{\partial u_g}{\partial t} = -\frac{1}{\rho} \frac{\partial p}{\partial x} + g \sin\alpha + \nu \frac{\partial^2 u_g}{\partial z^2}, \tag{3.1}$$

https://doi.org/10.1017/S0022112011000681 Published online by Cambridge University Press

where $u_g(x, z, t)$ denotes the fluid velocity, ρ is the density of water and $\nu = \mu/\rho$. Ignoring the velocity in the z-direction because of the narrowness of the gap, the pressure is independent of z coordinate. Moreover, the pressure gradient along the slide bottom is

$$\frac{\partial p}{\partial x} = \frac{p_b(X, t)}{X(t) - X_0(t)}, \tag{3.2}$$

where $p_b(X, t)$ can be evaluated from (2.5) and $X_0(t)$ is the cross-sectionally averaged trailing edge of the fluid in the gap, which must satisfy the following cross-sectionally averaged kinematic condition,

$$\frac{\mathrm{d}X_0}{\mathrm{d}t} = \frac{1}{\delta}\int_0^\delta u_g(x, z, t)\,\mathrm{d}z. \tag{3.3}$$

Note that $u_g(x, z, t)$ depends on x parametrically. For brevity, we suppress x from here on. The boundary conditions and the initial condition can be specified, respectively, as

$$u_g(0, t) = 0; \quad u_g(\delta, t) = \frac{\mathrm{d}X}{\mathrm{d}t} \quad \text{and} \quad u_g(z, 0) = 0. \tag{3.4}$$

We note that in this formulation we have ignored the dynamic effects of fluids entering the gap at the tip of the slide, $X(t)$, and the waterline dynamics in the vicinity of $X_0(t)$.

We first solve the initial boundary value problem for u_g in terms of $X(t)$ and $X_0(t)$. Let $u_g = u_o + U(z, t)$ with

$$u_o = \frac{\mathrm{d}X}{\mathrm{d}t}\frac{z}{\delta}, \tag{3.5}$$

which satisfies the inhomogeneous boundary condition. Then the governing equation for U becomes

$$\frac{\partial U}{\partial t} - \nu\frac{\partial^2 U}{\partial z^2} = Q(z, t) \equiv -\frac{1}{\rho}\frac{\partial p}{\partial x} + g\,\sin\alpha - \frac{z}{\delta}\frac{\mathrm{d}^2 X}{\mathrm{d}t^2}. \tag{3.6}$$

The boundary and initial conditions can also be reduced to

$$U = 0, \quad z = 0 \text{ and } \delta; \quad U(z, 0) = -\frac{\mathrm{d}X}{\mathrm{d}t}\frac{z}{\delta}. \tag{3.7}$$

The solution can be obtained by the eigenfunction expansion method. Thus,

$$U = \sum_1^\infty T_n(t)\sin\frac{n\pi z}{\delta}, \quad Q = \sum_1^\infty Q_n(t)\sin\frac{n\pi z}{\delta}, \quad U(z, 0) = \sum_1^\infty U_n \sin\frac{n\pi z}{\delta}, \tag{3.8}$$

where U_n are constants. For later use we have

$$Q_n = \frac{2}{\delta}\int_0^\delta \sin\frac{n\pi z}{\delta}\,\mathrm{d}z = \frac{4}{(2n-1)\pi}\left[-\frac{1}{\rho}\frac{p_b(X, t)}{X(t) - X_0(t)} + g\,\sin\alpha\right] - \frac{2(-1)^n}{n\pi}\frac{\mathrm{d}^2 X}{\mathrm{d}t^2}. \tag{3.9}$$

Then the ordinary differential equation and the initial condition for T_n become

$$\frac{\mathrm{d}T_n}{\mathrm{d}t} - \nu\frac{n^2\pi^2}{\delta^2}T_n = Q_n(t), \quad t > 0, \tag{3.10}$$

$$T_n(0) = U_n. \tag{3.11}$$

https://doi.org/10.1017/S0022112011000681 Published online by Cambridge University Press

The solution for T_n can be expressed as

$$T_n(t) = U_n e^{-\lambda_n t} + \int_0^t Q_n(t')\, e^{-\lambda_n (t-t')} dt', \quad \text{with } \lambda_n = \nu \frac{n^2\pi^2}{\delta^2}. \tag{3.12}$$

Finally, the velocity can be obtained as

$$u_g = \frac{dX}{dt}\frac{z}{\delta} + \sum_1^\infty \sin\frac{n\pi z}{\delta} T_n(t). \tag{3.13}$$

From (2.3), the lubrication resistance can be calculated as

$$F_h = \mu\,[X(t) - X_0(t)] \left[\frac{dX}{dt}\frac{1}{\delta} + \sum_1^\infty \frac{n\pi}{\delta}(-1)^n T_n(t)\right]. \tag{3.14}$$

Finally, we invoke (3.13) to get

$$\frac{dX_0}{dt} = \frac{1}{2}\frac{dX}{dt} + \sum_1^\infty \frac{2}{(2n-1)\pi} T_n(t). \tag{3.15}$$

From (2.5), (2.7)–(2.9), (3.13) and (3.15), six unknowns $\eta(x,t)$, $u(x,t)$, $p_b(x,t)$, $u_g(x,t)$, $X(t)$ and $X_0(t)$ can be calculated. Note that F_h is nonlinear in X and X_0. The nonlinear coupling between waves and the slide motion is not trivial. In this paper, we have developed a numerical algorithm solving the coupled nonlinear problem. The algorithm is presented in the Appendix.

4. Numerical examples – results and discussions

In this section, we present results for a falling solid slide of cosine profile

$$B = \frac{B_0}{2}\left[1 - \cos\left(\frac{2\pi}{L}\xi\right)\right], \quad 0 < \xi < L, \tag{4.1}$$

where B_0 measures the height of the slide. Our primary interest is to understand the effects of lubricative friction and solid friction on the wave generation process. Therefore, we fix the slope, $\alpha = 0.1$ (rad), the length of the slide, $L = 20$ m and the constant water depth $H_0 = 10$ m such that the generated waves are long waves, i.e. $H_0/L = 0.2$. The toe of the beach is 40 m from the still water shoreline. Finally, the ratio of the solid slide density to water density is also kept as a constant $\gamma_s = \rho_s/\rho = 2.0$.

In the first set of cases, the solid friction is ignored, i.e. $F_s = 0$ in (2.7). From (2.3) and (2.7), it is straightforward to estimate the relative importance of the lubricative frictional force to the gravity force as $O(F_h/[Mg\sin\alpha]) = O(\mu U_s/[\rho_s g B_0 \delta \sin\alpha])$. Clearly the importance of lubricative friction increases as the landslide speed increases and as the gap decreases. This observation is confirmed by the numerical results shown in figure 2, in which the force ratio, $F_h/(Mg\sin\alpha)$, is plotted for two different initial slide velocities, $U_s = 5$ and $10\,\mathrm{m\,s^{-1}}$, with three different gap thicknesses, $\delta = 10^{-2}, 10^{-3}$ and 10^{-4} m, respectively. In figure 3, the velocity profiles inside the gap, u_g, are plotted for three different gap sizes, $\delta = 10^{-2}, 10^{-3}$, and 10^{-4} m at three different times, $U_s t/L_0 = 0.1198,\ 0.2995,\ 0.4792$, where $U_s = 5\,\mathrm{m\,s^{-1}}$ and $B_0 = 0.5$ m are chosen. It is noticed that for smaller gap sizes, $\delta = 10^{-3}$ and 10^{-4} m, the velocity profiles are almost linear in z. This is not surprising. For these two cases, the shear stress dominates in (3.1), the flow inside the gap becomes a quasi-steady Couette flow, yielding a linear velocity profile with a slope of $(dX/dt)/\delta$. Note that because

https://doi.org/10.1017/S0022112011000681 Published online by Cambridge University Press

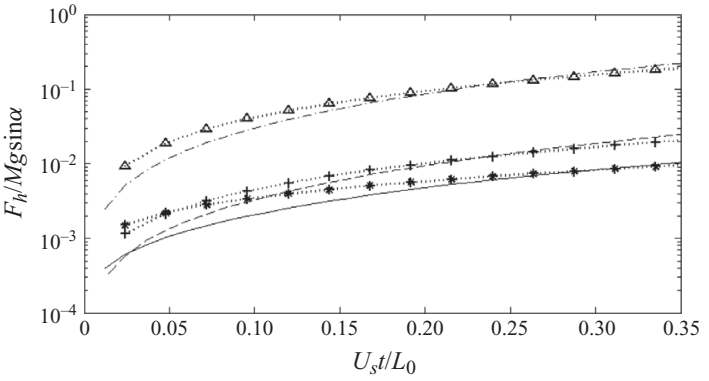


FIGURE 2. The ratio of lubricative force and gravity force. Two sets of results are shown. (*a*) $U_s = 5\,\mathrm{m\,s^{-1}}$: solid line ($\delta = 10^{-2}$ m); dashed line ($\delta = 10^{-3}$ m); dash-dotted line ($\delta = 10^{-4}$ m); (*b*) $U_s = 10\,\mathrm{m\,s^{-1}}$: $\triangle$ ($\delta = 10^{-4}$ m); ++ ($\delta = 10^{-3}$ m); $\diamond$ ($\delta = 10^{-2}$ m). In this figure, $B_0 = 0.5$ m and $f_s = 0$.

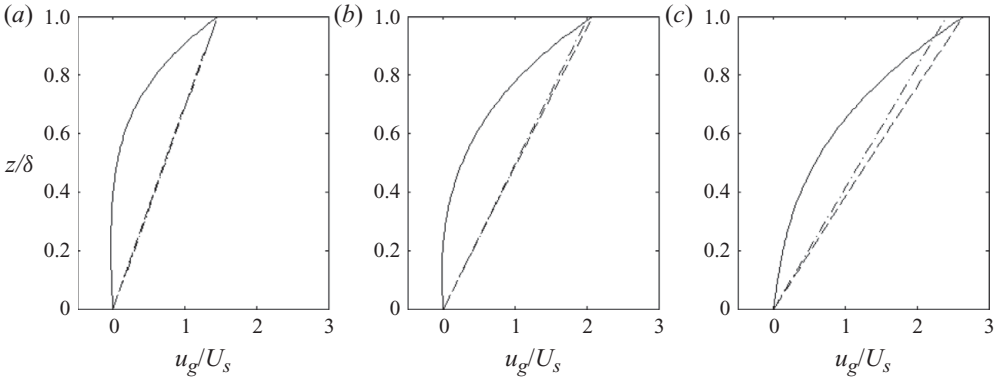


FIGURE 3. Snapshots of velocity profiles inside the gap at three different times. $U_s t/L_0 =$ (*a*) 0.1198; (*b*) 0.2995; (*c*) 0.4792. Results for three different gaps are plotted: solid line ($\delta = 10^{-2}$ m); dashed line ($\delta = 10^{-3}$ m); dash-dotted line ($\delta = 10^{-4}$ m). In this figure, $B_0 = 0.5$ m and $f_s = 0$.

of larger lubricative friction, the slide velocity, $\mathrm{d}X/\mathrm{d}t$, for the case of $\delta = 10^{-4}$ m is slightly slower than that for $\delta = 10^{-3}$ m. In the case of $\delta = 10^{-2}$ m, the dynamic pressure gradient is no longer negligible, the velocity profile deviates strongly from the linear one.

In figure 4, the time histories of the slide position, $X(t)$, and the tail of water inside the gap, $X_0(t)$, are plotted for the three cases shown in figure 3. For clarity the tail end of the slide, $X_{tail}(t) = X(t) - L$, is also shown. Note that $X_0 - X_{tail}$ represents the length of air in the gap. In the small gap cases, the flow velocity profiles are almost linear. Therefore, from (3.3) $X_0(t) \approx X(t)/2$. For the large gap case ($\delta = 10^{-2}$ m), $X_0(t) < X(t)/2$. Therefore, in all three cases, the air in the gap completely escapes before the slide is stopped at the toe of the slope. Recall that the slope length, L_0, is twice the slide length, L, in all examples given herein. Hence, in the small gap cases, the gap will be filled with water at the moment that the slide is stopped. With a smaller gap, the lubricative resistance is stronger and the slide moves slower. Consequently, it takes slightly longer time for the slide to reach the toe of the slope.

https://doi.org/10.1017/S0022112011000681 Published online by Cambridge University Press

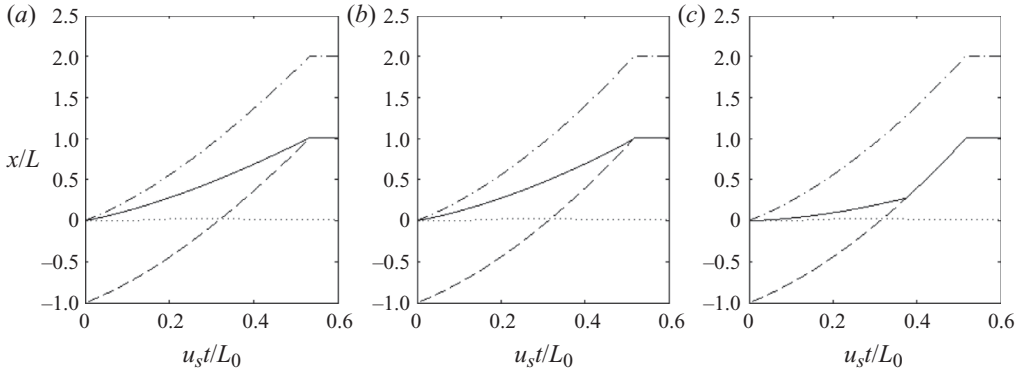


FIGURE 4. The instantaneous positions of the head of the slide $X(t)$ (dashed line), the tail of the slide $X_{tail}(t)$ (dashed line) and the air–water interface inside the gap $X_0(t)$ (Solid line) for three gap thicknesses: (*a*) $\delta = 10^{-4}$ m; (*b*) $\delta = 10^{-3}$ m; (*c*) $\delta = 10^{-2}$ m. In this figure, $U_s = 5\,\mathrm{m\,s^{-1}}$, $B_0 = 0.5$ m and $f_s = 0$.

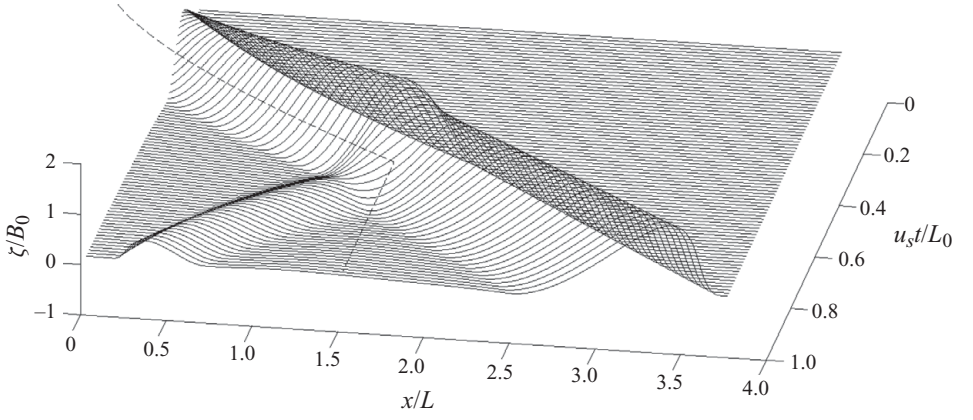


FIGURE 5. The evolution of surface profiles of waves generated by a solid slide with consideration of lubricative resistance. The dashed line indicates the location of the crest of the slide. In this figure, $U_s = 5\,\mathrm{m\,s^{-1}}$, $B_0 = 0.5$ m, $f_s = 0$ and $\delta = 10^{-4}$ m.

For the present cases, the slides stop at $t = 10.72$ s (or $U_s t/L_0 = 0.54$) for $\delta = 10^{-4}$ m, $t = 10.39$ s (or $U_s t/L_0 = 0.52$) for $\delta = 10^{-3}$ m, and $t = 10.37$ s (or $U_s t/L_0 = 0.52$) for $\delta = 10^{-2}$ m, respectively.

The evolution of surface profiles of generated waves for the case where $U_s = 5\,\mathrm{m\,s^{-1}}$, $B_0 = 0.5$ m, $f_s = 0$ and $\delta = 10^{-4}$ m is shown in figure 5. The dashed line indicates the location of the crest of the slide. During the initial stage as the solid slide enters into the water body, a leading elevated N-wave is generated above and moves with the slide. The shoreline retreats slightly into ocean during this stage. Once the slide is stopped, the seaward propagating wave continues its seaward propagation and a smaller elevated wave is generated, propagating in the shoreward direction. The overall features of water surface evolution for other two cases with larger gap sizes are very similar and, therefore, they are not presented here. Instead, snapshots of free surface profile at $U_s t/L_0 = 0.479$, 0.599 and 0.719 are presented in figure 6. It can be seen that the differences between the cases with $\delta = 10^{-2}$ and $\delta = 10^{-3}$ m are very small, while the waves generated in the case with $\delta = 10^{-4}$ m are slightly larger and

https://doi.org/10.1017/S0022112011000681 Published online by Cambridge University Press

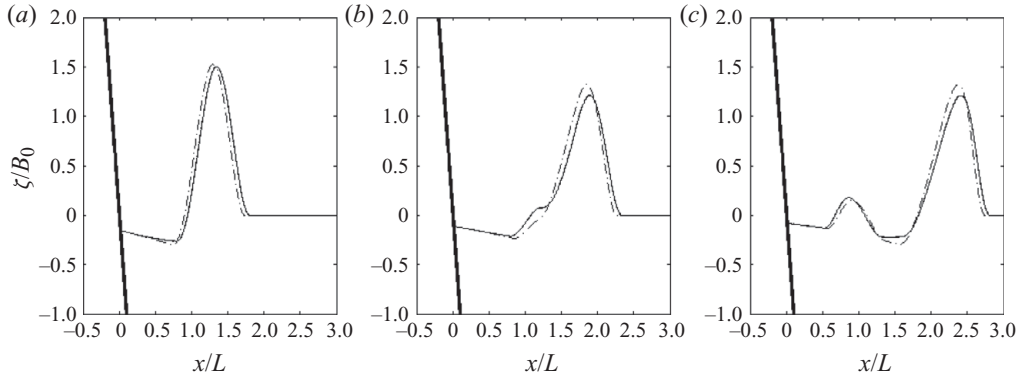


FIGURE 6. Snapshots of free surface profile at $U_s t/L_0 =$ (*a*) 0.479; (*b*) 0.599; and (*c*) 0.719 for different gap sizes: solid line ($\delta = 10^{-2}$ m); dashed line ($\delta = 10^{-3}$ m); dash-dotted line ($\delta = 10^{-4}$ m). For all three cases, $U_s = 5\,\mathrm{m\,s^{-1}}$, $B_0 = 0.5$ m and $f_s = 0$.

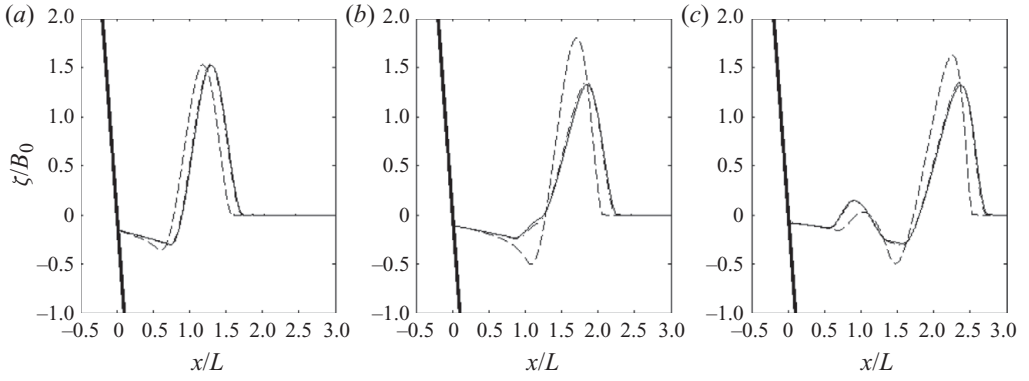


FIGURE 7. Snapshots of free surface profile at $U_s t/L_0 =$ (*a*) 0.479; (*b*) 0.599 and (*c*) 0.719 for different solid friction: solid line ($f_s = 0$); dash-dotted line ($f_s = 10^{-3}$); dashed line ($f_s = 10^{-2}$). For all plots $U_s = 5\,\mathrm{m\,s^{-1}}$, $B_0 = 0.5$ m and $\delta = 10^{-4}$ m.

moves with a slower speed. This is consistent with the fact that a stronger lubricative resistance slows down the slide speed and increases the duration of slide movement. The rundown of the shoreline can be seen in figure 6.

In the second set of examples, the effects of solid friction are considered. The case studied in the previous section, where $B_0 = 0.5$ m, $U_s = 5\,\mathrm{m\,s^{-1}}$ and $\delta = 10^{-4}$ m, is re-examined by adding solid friction with two different coefficients, $f_s = 10^{-2}$ and 10^{-3}. In figure 7, free surface profiles at $U_s t/L_0 = 0.479$, 0.599 and 0.719 for different solid friction coefficients, $f_s = 0$, 10^{-3} and 10^{-2}, are shown. The primary effect of the solid friction is to slow down the sliding mass. Therefore, with stronger solid friction, the slide moves with a slower speed and so does the generated wave. It is seen in the figure that results for $f_s = 10^{-3}$ are practically the same as those when solid friction is ignored. However, when the solid friction is increased to $f_s = 10^{-2}$, the generated waves are slower, but bigger.

Next we demonstrate the effects of landslide height. Two different slide heights with $B_0 = 0.1$ and 0.5 m are employed for comparison. For each slide height, two gap sizes are examined; $\delta = 10^{-3}$ and $\delta = 10^{-4}$ m. Snapshots of free surface profiles at $U_s t/L_0 = 0.9$ are plotted in figure 8. Note that the free surface elevation is normalized

https://doi.org/10.1017/S0022112011000681 Published online by Cambridge University Press

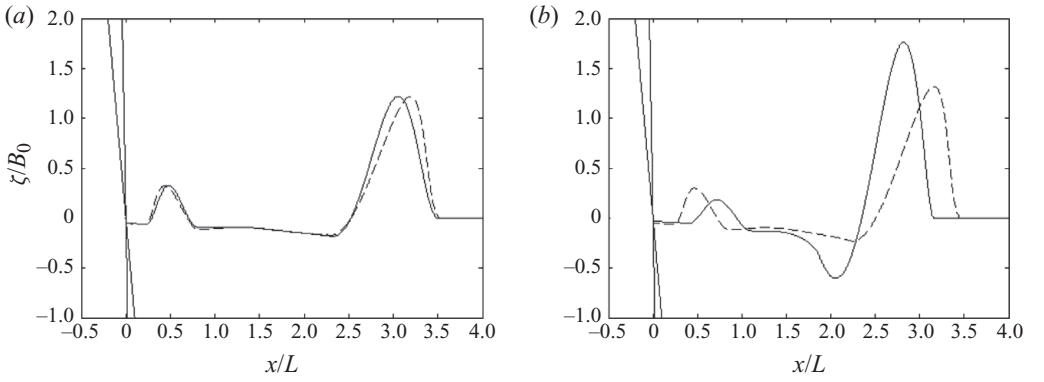


FIGURE 8. Snapshots of free surface profile at $U_s t/L_0 = 0.9$ for B_0 and δ. (*a*) $\delta = 10^{-3}$ m and (*b*) $\delta = 10^{-4}$ m. The dashed line is for $B_0 = 0.1$ m and the solid line for $B_0 = 0.5$ m. For both plots $U_s = 5\,\mathrm{m\,s^{-1}}$ and $f_s = 0$.

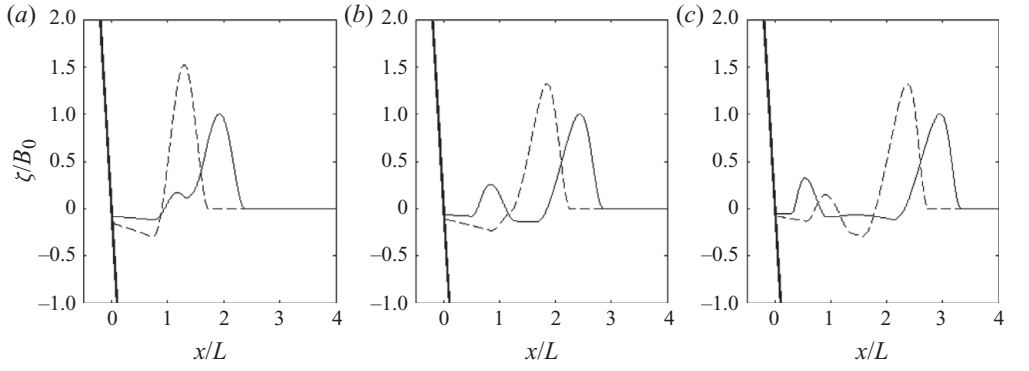


FIGURE 9. Snapshots of free surface profile at $U_s t/L_0 =$ (*a*) 0.479; (*b*) 0.599 and (*c*) 0.719 for different initial slide speeds: solid line ($U_s = 10\,\mathrm{m\,s^{-1}}$); dashed line ($U_s = 5\,\mathrm{m\,s^{-1}}$). For all three plots, $B_0 = 0.5$ m, $f_s = 0$ and $\delta = 10^{-4}$ m.

by the slide height in this figure. For the case with a weaker lubricative resistance ($\delta = 10^{-3}$ m), the amplitude of generated wave scales linearly with the slide height. The higher slide generates a wave with steeper front. On the other hand, when the lubricative resistance is stronger ($\delta = 10^{-4}$ m), the generated wave moves with slightly slower speed with a much larger amplitude and steeper front.

Figure 9 compares free surface profiles for waves generated by slides with different initial velocities: $U_s = 10\,\mathrm{m\,s^{-1}}$ and $U_s = 5\,\mathrm{m\,s^{-1}}$, respectively. In both cases $B_0 = 0.5$ m, $f_s = 0$ and $\delta = 10^{-4}$ m are considered. In the figure snapshots of free surface profiles at $U_s t/L_0 = 0.479$, 0.599 and 0.719 are plotted. Once again since the generated wave moves with the slide before the slide stops at the toe of the slope, the slide with faster initial speed generates a faster moving, but smaller wave.

5. Concluding remarks

Up to now in most of the existing numerical models for studying landslide generated waves the slide speed is prescribed. This paper advances the modelling of solid landslide generated water waves in laboratory by including the coupling between solid slide motion and water wave dynamics. The present model for slide

https://doi.org/10.1017/S0022112011000681 Published online by Cambridge University Press

movement considers solid friction, lubricative resistance and hydrodynamic pressure force. Numerical examples are provided to illustrate the effects of different resistances and the size and the initial speed of the slide on generated waves. The present approach adopts the nonlinear shallow water equations to describe the wave hydrodynamics and can be extended to 2D horizontal problem, in which a 3D slide can be studied. Finally one can use the Boussinesq equations if the dispersion effects need to be considered.

The research presented here is supported by grants from National Science Foundation to Cornell. C.C.M. thanks the Mary Upson Visiting Professorship from Cornell which made this collaboration possible. Y.W. was supported by a Chinese Government Scholarship.

Appendix. Numerical algorithm

The continuity and momentum equations, (2.8) and (2.9), are solved by the explicit leap-frog finite difference method developed by Liu *et al.*(1995). Since the coupled problem is nonlinear, an iterative scheme is developed within each time step, which is outlined as follows.

(i) At the end of the previous time step computation, the following quantities have been obtained: X^k, X_0^k, $\dot{X}^k$, q^k, p_b^k, $\ddot{X}^{k-1/2}$, $\dot{X}^{k-1/2}$, $\eta^{k-1/2}$, where $q=(\eta+H-B)u$ and k represents the kth time step. The continuity equation (2.8) is solved by a forward finite difference method to find the free surface elevation at the $(k+1/2)$th time step, i.e. $\eta^{k+1/2}$.

(ii) To initiate the iteration at the $k+1$ time level the following estimations are first made: $X^{k+1,(0)}=\dot{X}^k\Delta t+X^k$; $X_0^{k+1,(0)}=X_0^k$; $\ddot{X}^{n+1/2,(0)}=\ddot{X}^{n+1/2}$; $\dot{X}^{n+1/2,(0)}=\dot{X}^{n+1/2}$, where Δt is the time step size and the superscript (0) denotes the initial estimate in the iterative scheme.

(iii) For (i)th iteration, we approximate $X^{k+1/2,(i)}=(X^{k+1/2,(i-1)}+X^k)/2$; $X_0^{k+1/2,(i)}=(X_0^{k+1/2,(i-1)}+X_0^k)/2$.

(iv) Equation (2.5) is used to calculate $p_b^{k+1/2,(i)}$ and (2.6) to find $x_c^{n+1/2,(i)}$.

(v) Using $p_b^{k+1/2,(i)}$ and $\ddot{X}^{n+1/2,(i-1)}$, we find $Q_n^{n+1/2,(i)}$ from (3.9), $T_n^{k+1/2,(i)}$ from (3.12) and $U^{k+1/2,(i)}$ from (3.8).

(vi) Equation (3.5) is used to calculate $u_o^{k+1/2,(i-1)}$, (3.13) for $u_g^{k+1/2,(i)}$ and (3.14) for $F_h^{k+1/2,(i)}$.

(vii) The equation for slide motion, (2.7), is used to find $\ddot{X}^{k+1/2,(i)}$, which yields $X^{k+1,(i)}=X^k+\Delta t(\dot{X}^k+\ddot{X}^{k+1/2,(i)}\Delta t/2)$; $\dot{X}^{k+1/2,(i)}=\dot{X}^k+\Delta t\ddot{X}^{k+1/2,(i)}/2$.

(viii) $X^{k+1/2,(i)}$ and $u_g^{k+1/2,(i)}$ are used to calculate $X_0^{k+1,(i)}$ from (3.3).

(ix) A convergence condition for the relative error of all variables is imposed. If the convergence condition is not satisfied, the new $X^{k+1/2,(i)}$ is used to repeat the process starting from the first iterative step.

(x) If the convergence condition is satisfied, $X^{k+1/2}$ and $\ddot{X}^{k+1/2}$ are used to march forward in time to find $\dot{X}^{k+1}$ and X^{k+1}.

(xi) The momentum equation (2.9) is solved to find the velocity field u^{k+1} and the volume flux q^{k+1}.

(xii) The slide motion is stopped when the tip of the slide reaches the toe of the slope. Equations (2.8) and (2.9) are used to propagate waves in both seaward and shoreward directions.

https://doi.org/10.1017/S0022112011000681 Published online by Cambridge University Press

REFERENCES

Liu, P. L.-F., Cho, Y.-S., Briggs, M. J., Kanoglu, U. & Synolakis, C. E. 1995 Runup of solitary waves on a circular island. *J. Fluid Mech.* **302**, 259–285.

Liu, P. L.-F., Lynett, P. & Synolakis, C. E. 2003 Analytical solutions for forced long waves on a sloping beach. *J. Fluid Mech.* **478**, 101–109.

Liu, P.-F., Wu, T.-R., Raichlen, F., Synolakis, C. E. & Borrero, J. C. 2005 Runup and rundown generated by three-dimensional sliding masses. *J. Fluid Mech.* **536**, 107–144.

Lynett, P. & Liu, P. L.-F. 2002 A numerical study of submarine-landslide-generated waves and run-up. *Proc. R. Soc. Lond.* A **458**, 2885–2910.

Lynett, P. & Liu, P. L.-F. 2005 A numerical study of the runup generated by three dimensional landslides. *J. Geophys. Res.* **110**, doi:10.1029/2004JC002443.

Pelinovsky, E. & Poplavasky, A. 1996 Simplified model of tsunami generation by submarine landslide. *Phys. Chem. Earth* **21** (12), 13–17.

Renzi, E. & Sammarco, P. 2010 Landslide tsunami propagating around a conical island. *J. Fluid Mech.* **650**, 250–285.

Sammarco, P. & Renzi, E. 2008 Landslide tsunami propagating along a plane beach. *J. Fluid Mech.* **598**, 107–119.

Synolakis, C. E., Bardet, J. P., Borrero, J., Davies, H., Okal, E. A., Silver, E. A., Sweet, S. & Tappin, D. R. 2002 Slump origin of 1998 Papua New Guinea tsunami. *Proc. R. Soc. Lond.* A **458**, 736–789.

Tinti, S., Pagnoni, G., Zaniboni, F. & Bortolucci, E. 2003 Tsunami generation in Stromboli island and impact on the south-east Tyrrhenian coasts. *Nat. Hazards Earth Syst. Sci.* **3**, 299–309.

Watts, P., Grilli, S. T., Kirby, J. T., Fryer, G. J. & Tappin, D. R. 2003 Landslide tsunami case studies using a Boussinesq model and a fully nonlinear tsunami generation model. *Nat. Hazards Earth Syst. Sci.* **3**, 391–402.

https://doi.org/10.1017/S0022112011000681 Published online by Cambridge University Press